Polymorphism and bistability in adherent cells

Shiladitya Banerjee[1] and Luca Giomi[2, 3]

[1] *Department of Physics, Syracuse University, Syracuse, New York 13244, USA*
[2] *School of Engineering and Applied Sciences, Harvard University, Cambridge, Massachusetts 02138, USA*
[3] *International School for Advanced Studies (SISSA), Via Bonomea 265, 34136 Trieste, Italy*

The optimal shapes attained by contractile cells on adhesive substrates are determined by the interplay between intracellular forces and adhesion with the extracellular matrix. We model the cell as a contractile film bounded by an elastic cortex and connected to the substrate via elastic links. When the adhesion sites are continuously distributed, optimal cell shape is constrained by the adhesion geometry, with a spread area sensitively dependent on the substrate stiffness and contractile tension. For discrete adhesion sites, equilibrium cell shape is convex at weak contractility, while developing local concavities at intermediate values of contractility. Increasing contractility beyond a critical value, controlled by mechanical and geometrical properties of adhesion, cell boundary undergoes a discontinuous transition to a star-shaped configuration with cusps and protrusions, accompanied by a region of bistability and hysteresis.

INTRODUCTION

Mechanical force generation during cell-matrix adhesion is strongly influenced by the ability of cells to actively probe the mechanical and geometrical cues in the extracellular matrix [1]. Matrix stiffness plays a profound role in regulating a variety of cellular processes, from morphogenesis, motility to cell spreading and cytoskeletal activity. Cells adhering to softer substrates spread less and prefer to have well rounded morphologies, while they are more likely to exhibit branched patterns on stiffer substrates with greater spread area [2, 3]. Experiments on micro-patterned adhesive islands revealed that cell fate, proliferation and spreading sensitively depend on adhesion geometry [4]. However, cellular response to extracellular determinants is strongly linked to myosin dependent activity of the cell cytoskeleton [5]. While myosin activity can influence force transmission by regulating the growth of focal adhesions [6], it can also drive changes in cell morphology, as seen by pharmacologically disrupting the cell cytoskeleton [7] or by inhibiting myosin-II activity [8]. Traction forces exerted by cells on substrates can now be determined accurately using traction force microscopy or micropillar assays [9, 10], but the intimate relation between cell shape and traction mechanics requires further quantitative investigation. In this article we present a minimal mechano-geometric model for isolated adherent cells that addresses a fundamental question in cell mechanics and morphogenesis: How intercellular and extracellular forces cooperate to control the geometry of cell shapes? At time scales when the cell is fully spread and develops stronger focal adhesions, the dominant forces in the cell stem from surface tension induced by actomyosin contractility and elasticity in the actin rich cortex. These intracellular forces act in opposition to receptor-mediated adhesive forces in determining optimal cell shapes [11, 12]. Although chemical pathways can trigger a feedback between cell activity and cell-substrate adhesion [13], we instead focus on their mechanical cooperativity in regulating cell shapes. Tuning stiffness of the matrix and acto-myosin contractility, we discuss how cells can be driven through a series of morphological transitions - convex, concave, cusps and protrusions with associated hysteresis. In addition, we provide several analytical results relating geometrical properties of cells e.g. curvature, spread radius to mechanical properties such as substrate stiffness and contractile surface tension, that are amenable to experimental verification and quantitative comparison.

CONTRACTILE FILM MODEL FOR ADHERENT CELLS

We consider a planar adherent cell subject to internal contractile forces. The shape of the cell is parametrized by the contour $\boldsymbol{r}(s)$, where s represents arc-length. The total mechanical energy of the stationary cell is given by:

$$E = \sigma \int dA + \alpha \oint ds\, \kappa^2 + k_s \oint ds\, \rho \left| \boldsymbol{r} - \boldsymbol{r}_0 \right|^2 , \quad (1)$$

where σ is the *effective* surface tension in the cell due to acto-myosin contractility, κ is the local curvature of the cell boundary and α the associated bending rigidity. The last term in Eq. (1) represent the strain energy induced by the cell on a substrate of stiffness k_s through focal adhesions localized at the cell edge [14] with density $\rho(s)$, so that the total number of adhesions is $N_A = \oint ds\rho$. The reference configuration $\boldsymbol{r}_0(s)$ describes the shape attained by the cell boundary on a rigid substrate, and is a constraint set by the adhesion geometry. The assumption of local elastic interaction with the substrate is strictly relevant for cells cultured on elastomeric pillars or on continuous substrates of depth thinner than cell perimeter. From a purely mechanical point of view, the Contractile Film Model defined by Eq. (1) is equivalent to a fluid film bounded by a planar *Elastica* [15, 16] and attached to a continuous or discrete set of links to a compliant substrate. Unlike other models of softly restrained films [17–21], Eq. (1) does not involve any constraint on the perimeter of the cell, which is then only *softly constrained*

by the adhesion with the substrate. In the special case of constant curvature, Eq. (1) reduces to the model introduced in Ref. [7, 22, 23], with an effective line tension $\lambda = \alpha\kappa^2$. As we will see below, this assumption holds exclusively when adhesions are uniformly distributed along the cell boundary, thus forcing the curvature itself to be uniform, while in the case of discrete adhesions κ is always non-uniform.

Continuous adhesions. In this case the periphery of the cell forms contact with a single continuous adhesion site, so that $\rho = 1/\mathcal{L}$ with $\mathcal{L} = \oint ds$ the perimeter of the cell. In presence of a uniform and isotropic substrate, we can assume the reference configuration to be a circle of radius R_0 so that a natural minimizer of the energy (1) would be a circle or radius R. Minimizing Eq. (1) with respect to R yields the following cubic equation:

$$(k_s + \pi\sigma)R^3 - k_s R_0 R^2 - \pi\alpha = 0 , \quad (2)$$

The equation contains two length scales, R_0 and $\xi_\sigma = (\alpha/\sigma)^{1/3}$, and a dimensionless control parameter k_s/σ expressing the relative amount of adhesion and contraction. For very soft anchoring $k_s \ll \sigma$ and Eq. (2) admits the solution $R = \xi_\sigma$, whereas if the cell is rigidly pinned at adhesion sites, $k_s \gg \sigma$ and $R \to R_0$. For intermediate values of k_s/σ the optimal radius R interpolates between ξ_σ and R_0 and is an increasing function of the substrate stiffness k_s, in case $\xi_\sigma < R_0$, or a decreasing function if $\xi_\sigma > R_0$. For $\xi_\sigma = R_0$, the lower and upper bound coincide, and the solution is $R = R_0$. In particular, the case $R_0 > \xi_\sigma$ reproduces the experimentally observed trend that cell projected area increases with increasing substrate stiffness before reaching a plateau at higher stiffnesses [2, 3]. We fit the solution to Eq. (2) to the measured data for projected areas of 3T3 fibroblasts adhering to densely spaced pillar arrays of varying stiffnesses [24], as shown in Fig. 1a. The fitted value for surface tension $\sigma = 2.7$ nN/μm comes to the same order of magnitude as reported for endothelial cells [23, 25] and epithelial cells [26]. The fit also provides a value for the bending rigidity $\alpha = 1.2 \times 10^{-19}$ Nm^2, of the same order of magnitude as estimated for actin cortex [27]. The asymptotic behavior and various limits of the solution are well captured by the interpolation formula:

$$R \approx \frac{k_s R_0 + 3\pi\sigma\,\xi_\sigma}{k_s + 3\pi\sigma} \quad (3)$$

indicating that larger surface tension, hence larger cell contractility σ leads to lesser spread area, consistent with the experimental observation that myosin-II activity retards the spreading of cells [28]. Standard stability analysis of this solution under a small periodic perturbation in the cell radius shows that the circular shape is always stable for any values of the parameters σ, k_s and R_0.

Discrete adhesions. For cells adhering to discrete number of adhesion sites, one can show that the circular
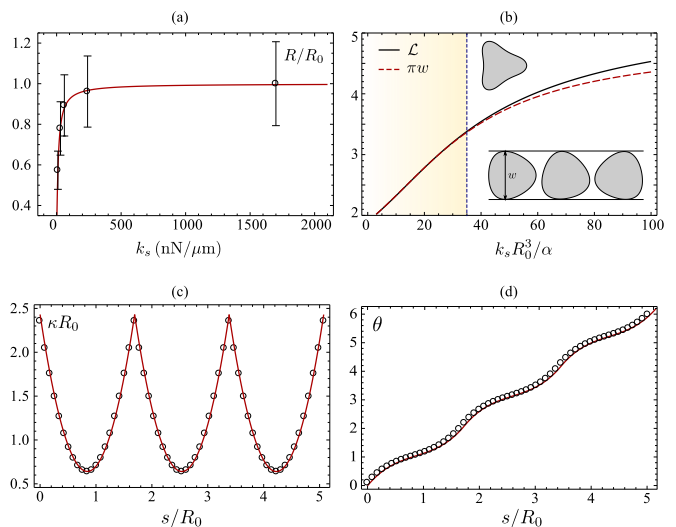

FIG. 1. *Geometric properties of an adherent cell.* (a) Relative cell radius R/R_0 as a function of substrate stiffness k_s for a 3T3 cell cultured on pillar arrays [24] (black). Cell radius is estimated from area reported in [24] as $R = \sqrt{\text{area}/\pi}$. Solid (red) line represents the solution to Eq. (2) with $\sigma = 2.7$ nN/μm and $\alpha/R_0^3 = 0.06$ nN/μm. (b) The total cell length $\mathcal{L}$ as a function of adhesion stiffness. For small stiffnesses the cell boundary form a curve of constant width (lower inset) and $\mathcal{L} = \pi w$, with w the width of the curve. This property breaks down for larger stiffnesses when inflection points develops (upper inset). The curvature (c) and the tangent angle (d) as function of arc-length for $\sigma R_0^3/\alpha = 10$, $k_s R_0^3 = 50$ and $N_A = 3$. The circle are obtained from a numerical minimization of a discrete version of the energy (1), while the solid lines are obtained respectively from our analytical approximation.

solution for the cell boundary is never stable and there is always a non-circular configuration with lower energy. For simplicity, we assume that N_A adhesion sites are located at the vertices of a regular polygon of circumradius R_0, with density $\rho(s) = \sum_{i=0}^{N_A-1} \delta(s - iL)$, and L the distance between subsequent adhesions. Minimal cell shape is given by the solution to Euler-Lagrange equation obtained by minimizing the total energy in (1). It reads :

$$\alpha\left(2\kappa'' + \kappa^3\right) - \sigma + 2k_s \sum_{i=0}^{N_A-1} \delta(s - iL)\,(\boldsymbol{r} - \boldsymbol{r}_0) \cdot \boldsymbol{n} = 0 . \quad (4)$$

Here prime denotes derivative with respect to arc-length s and $\boldsymbol{n} = \boldsymbol{r}''/|\boldsymbol{r}''|$ is the normal vector. Due to the N_A-fold symmetry of the adhesion sites, adhesion springs stretch by an equal amount Δ in the direction of the normal vector: $(\boldsymbol{r}_i - \boldsymbol{r}_{0i}) \cdot \boldsymbol{n}_i = \Delta$, $i = 1, 2 \ldots N_A$. As a consequence of the localized adhesion forces, the curvature is non-analytical at the adhesion points. Integrating Eq. (4) along an infinitesimal neighborhood of a generic adhesion point i, one finds:

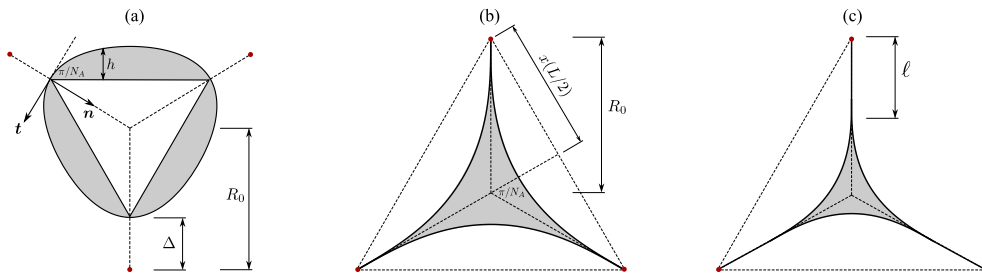$$\kappa'_i = -\frac{k_s}{2\alpha}\,\Delta . \quad (5)$$

FIG. 2. *Schematic of cell shapes.* (a) $\sigma < \sigma_{c1}$, cell contour is everywhere convex with constant width. (b) $\sigma = \sigma_p$, cell contour is purely concave with cusps at adhesion points and without protrusions. (c) $\sigma > \sigma_{c2}$, cusps are connected to the substrate by means of a protrusion of length ℓ.

The local curvature of the segment lying between adhesion points is on the other hand determined by the equation, $\alpha \left(2\kappa'' + \kappa^3\right) - \sigma = 0$, with boundary conditions : $\kappa(iL) = \kappa((i+1)L) = \kappa_0$. Without loss of generality we consider a segment located in $s \in [0, L]$. Although an exact analytic solution to the nonlinear equation for curvature is available (see Ref. [19] and *Supporting Information*), an excellent approximation can be obtained by neglecting the cubic nonlinearity (Fig. 1c-d). With this simplification, Eq. (4) admits a simple solution of the form:

$$\kappa(s) = \kappa_0 + \frac{\sigma}{4\alpha} s(s - L) . \quad (6)$$

Eqs. (6) and (5) immediately allow us to derive a condition on the cell perimeter: $L = 2k_s\Delta/\sigma$. Furthermore, the latter condition leads to a linear relation between traction force $T = 2k_s\Delta$, and cell size :

$$T = \sigma L , \quad (7)$$

which is indeed observed in traction measurements on large isolated cells [26].

To determine the end-point curvature κ_0, we use the turning tangents theorem for a simple closed curve [29], which requires $\int_0^L ds\, \kappa = 2\pi/N_A$. This leads to following relation between local curvature and segment length, or equivalently traction force, at the adhesion sites :

$$\kappa_0 = \frac{\sigma L^2}{24\alpha} + \frac{2\pi}{N_A L} = \frac{T^2}{24\,\alpha\sigma} + \frac{2\pi\sigma}{N_A T} . \quad (8)$$

Finally, to determine the optimal length of the cell segment L, we are going to make use of a remarkable geometrical property of the curve obtained from the solution of Eq. (4) with discrete adhesions: the fact of being a *curve of constant width* [29]. The width of a curve is the distance between the uppermost and lowermost points on the curve (see lower inset of Fig. 1b). In general, such a distance depends on how the curve is oriented. There is however a special class of curves, where the width is the same regardless of their orientation. The simplest example of a curve of constant width is clearly a circle, in which case the width coincides with the diameter. A fundamental property of curves of constant width is

given by the Barbier's theorem [29], which asserts that the perimeter $\mathcal{L}$ of any curve of constant width is equal to width w multiplied by π: $\mathcal{L} = \pi w$. As illustrated in Fig. 1d, this is confirmed by numerical simulations for low to intermediate values for contractility and stiffness. With our setting, the cell width is given by:

$$w = (R_0 - \Delta)(1 + \cos \pi/N_A) + h(L/2) , \quad (9)$$

where $h(s) = \int_0^s ds'\, \sin\theta(s')$ is the height of the curve above a straight line connecting subsequent adhesions and

$$\theta(s) = \int_0^s ds'\, \kappa(s') = \theta_0 + \kappa_0 s + \frac{\sigma}{24\alpha} s^2(2s - 3L) \quad (10)$$

the angle formed by the tangent vector with the $x-$axis of a suitable oriented Cartesian frame (Fig. 2a). For small angles h can be approximated as : $h(s) \approx s(L - s)\left[\pi/(N_A L) - (\sigma/48\alpha)\, s(L - s)\right]$. Using this together with Eq. (9) and the Barbier's theorem with $\mathcal{L} = N_A L$ allow us to obtain a quartic equation for the cell length and the traction force, whose approximate solution is given by:

$$T \simeq \frac{\sigma R_0}{\left(g_0 + \frac{\sigma}{2k_s}\right)\left[1 + \frac{7\sigma R_0^3}{\alpha g_1}\left(g_0 + \frac{\sigma}{2k_s}\right)^{-4}\right]^{1/7}} , \quad (11)$$

where, $g_0 = (4N_A^2 - \pi^2)/[4\pi N_A(1 + \cos \pi/N_A)]$ and $g_1 = 768(1 + \cos \pi/N_A)$. Eq. (11) supports the experimental trend that traction force increases monotonically with substrate stiffness k_s before plateauing to a finite value for higher stiffnesses [24, 30]. The plateau value increases with increasing contractility (Fig. 3a). Traction force grows linearly with increasing contractility for $\sigma R_0^3/\alpha \ll 1$, before saturating to the value $2k_s R_0$ at large contractility $\sigma R_0^3/\alpha \gg 1$, as shown in Fig. 3b. Eq. (11) is also consistent with experimentally observed trend that reducing contractility by increasing the dosage of myosin inhibitor Blebbistatin, leads to monotonic drop in traction forces [30].

INFLECTIONS, CUSPS AND PROTRUSIONS

For low to intermediate values of σ and k_s, cell shape is convex and has constant width. Upon increasing σ above a k_s−dependent threshold σ_{c1}, however, the cell boundary becomes inflected (see Fig. 4 and upper inset of Fig. 1b). Initially a region of negative curvature develops in proximity of the mid point between two adhesions, but as the surface tension is further increased, the size of this region grows until positive curvature is preserved only in a small neighborhood of the adhesion points. Due to the presence of local concavities, the cell boundary is no longer a curve of constant width. Convex and concave regions are separated by inflection points, given by the solution to $\kappa = 0$, or explicitly: $s^2 - Ls + 4\alpha\kappa_0/\sigma = 0$. In order for this equation to have real solutions one needs $\sigma L^3 > 96\pi\alpha/N_A$. Fig. 3d shows σ_{c1} as a function of k_s.

Upon increasing σ above a further threshold value σ_{c2}, the inflected shape collapses giving rise to the star-shaped configurations shown in upper right corner of Fig. 4. These purely concave configurations are made by arcs whose ends meet in a cusp. The cusp is then connected to the substrate by a protrusion consisting of a straight segment of length ℓ that extends until the adhesion point rest position, so that $\Delta \approx 0$ (Fig. 2c) (see *Supporting Information*). The cell boundary becomes pinned at adhesion sites as a result of having to satisfy force-balance (Eq. (4)) and adhesion-induced boundary condition (Eq. (5)), while accommodating large contractile tensions at its neighbourhood. This results in spontaneous expansion in the cell perimeter. Unlike the previous transition from convex to non-convex shapes, this second transition occurs discontinuously and is accompanied by a region of bistability in the range $\sigma_p < \sigma < \sigma_{c2}$. This is clearly visible in the hysteresis diagram in Fig. 3c showing the optimal length obtained by numerically minimizing a discrete analog of Eq. (1) in a cycle and using as initial configuration the output of the previous minimization. The onset of bistability is regulated by substrate stiffness as shown in Fig. 3d, with stiffer substrates promoting transition to cusps at lower σ_{c2}.

At $\sigma = \sigma_p$ the protrusion have zero length and the corresponding configuration of the cell boundary form a special curve from which all the shapes having non-zero protrusion length can be constructed by means of a *similarity* transformation. To see this let us set $\ell = 0$ at $\sigma = \sigma_p$ so that the shape of the cell will be of the kind illustrated in Fig. 2b. The approximated expression for the curvature is the same given in Eq. (6), but with $\Delta = 0$ and κ' unconstrained since the last term in Eq. (4) vanishes identically. The quantities κ_0 and L are left to determine. A first condition can be obtained by observing that: $x(L/2) = R_0 \sin \pi/N_A$, where $x(s)$ is the projection of the curve on the edge of the circumscribed polygon (see Fig. 2b). A second condition is given by the theorem of turning tangents for a simple closed curve with N_A cusps: $\int_0^L ds\, \kappa = \pi(2 - N_A)/N_A$. In the case $N_A = 3$, for instance, the right-hand side is equal to
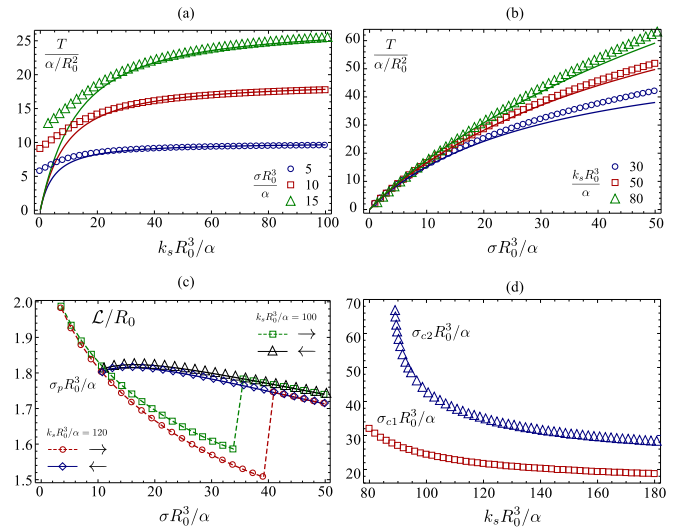

FIG. 3. *Substrate stiffness and cell contractility control traction forces and the stability of cell shapes.* Traction force as a function of substrate stiffness (a) and contractility (b) obtained from a numerical minimization of a discrete analog of Eq. (1). Solid curves denote the approximate traction values obtained from Eq. (11). (c) Boundary length $\mathcal{L}$ obtained by increasing (squares) and then decreasing (triangles) the contractility for substrate stiffnesses $k_s R_0^3/\alpha = 100$ (green squares, black triangles) and $k_s R_0^3/\alpha = 120$ (red squares, blue triangles). The diagram shows bistability in the range $\sigma_p < \sigma < \sigma_{c2}$. (d) The critical contractility σ_{c1} and σ_{c2} as functions of substrate stiffness.

$-\pi/3$, corresponding to the fact that the tangent vector rotates clockwise by $60°$ as we move counterclockwise along the curve from one cusp to the next. These allow us to calculate the *reference shape* shown in Fig. 2b. To determine σ_p we use the condition $\kappa_0 = 0$, below which the curvature turns everywhere negative. An analytical estimate for σ_p can be obtained by approximating $x(s)$ for small deviations about a flat segment. This gives us:

$$\sigma_p \simeq \frac{3\alpha\pi^4}{R_0^3 \sin^3 \frac{\pi}{N_A}} \left(\frac{N_A - 2}{N_A}\right)^4 . \tag{12}$$

Next, following Ref. [17, 20], we notice that the force balance equation $2\kappa'' + \kappa^3 - \sigma/\alpha = 0$ is invariant under the scaling transformation:

$$(s, \kappa, \sigma) \to \left(\lambda s, \frac{\kappa}{\lambda}, \frac{\sigma}{\lambda^3}\right) . \tag{13}$$

Consequently, the equilibrium shape obtained for a given value of $\sigma > \sigma_p$ are similar to the reference shape with a scaling factor $\lambda = (\sigma_p/\sigma)^{1/3} < 1$. Accordingly, the closed curve is rescaled so that $L = \lambda L_p$ and $A = \lambda^2 A_p$ with L_p and A_p respectively the length and the area of the reference shape. This beautiful geometric property immediately translates into the following algorithm to construct shapes with protrusion (Fig. 2c): *1)* Given the surface tension $\sigma > \sigma_p$ we calculate the scaling factor λ.
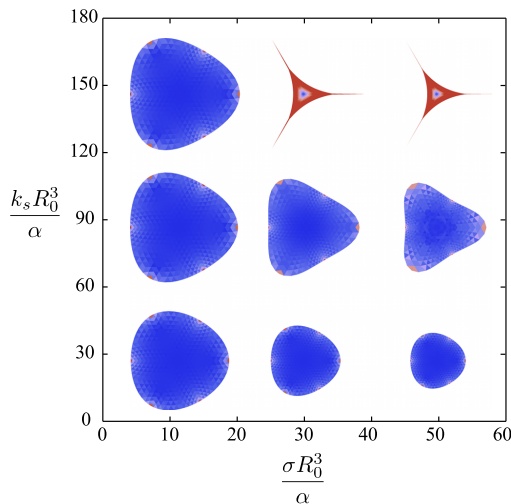
FIG. 4. *Cell Polymorphism.* Phase diagram in σ-k_s plane showing optimal configuration obtained by numerical minimization of the energy (1) for $N_A = 3$.

2) We rescale the reference curve so that $L = \lambda L_p$. *3)* Finally, we fill the distance between the adhesion points and the cusps with straight segments of length $\ell = R_0(1 - \lambda)$ (since R_0 is the circumradius of the reference shape and λR_0 that of the rescaled shape). This latter step, ultimately allows us to formulate a scaling law for the length of protrusions that can be tested in experiments:

$$\ell/R_0 = 1 - (\sigma_p/\sigma)^{1/3} . \quad (14)$$

This transition from a smooth shape to a self-contacting shape with cusps is reminiscent of the post-buckling scenario of an elastic ring subject to a uniform pressure [20]. But unlike this phenomenon, where the system undergoes a continuous transition from a simple curve to a curve with lines of contact, here the transition is discontinuous along both the loading branch (increasing k_s) and the unloading branch (decreasing k_s). The transition has moreover a strong topological character since it involves a jump in the turning number $(1/2\pi) \oint ds \, \kappa$.

DISCUSSION

The Contractile Film Model is limited to the steady state cell shapes and does not account for the dynamic feedback loop between cytoskeleton and focal adhesions during early stages of cell spreading and adhesion. The model provides a quantitative framework to describe how polymorphic cell shapes arise by tuning substrate stiffness, adhesion geometry and cell activity. The presence of bending deformations in the cell periphery naturally allows for optimal cell shapes with non-uniform boundary curvatures, a feature not included in previous theoretical works on cell shapes [7, 22, 23]. Bending in the cell boundary can also arise due to splay deformations in

the Arp2/3 regulated actin array in the lamellipodium. Although our model relies on local mechanotransduction through adhesions localized at the cell edge, in reality traction stresses penetrate inside the cell up to a characteristic depth controlled by cellular and substrate stiffness [26]. Our model is thus applicable to cell sizes much larger than traction penetration depth and predicts the same trend on the dependence of traction forces on substrate stiffness as derived using long-range elastic models [31]. Although, local mechanosensing at cell periphery coupled with global surface tension due to cytoskeletal contractility can accurately capture experimental trends for cell size and traction forces, the effect of non-local interactions of the cytoskeleton with the substrate cannot be neglected at actin remodeling time scales.

An important consequence of increasing surface tension is the loss of stability of smooth shapes and a discontinuous transition to cusps and protrusion (Fig. 3 and 4). The transition is favored on stiffer substrates (see Fig. 4) and leads to spontaneous expansion in the cell perimeter and relaxation of localized adhesion springs. Such a transition could also possibly occur on cellular timescales via chemo-mechanical instabilities induced by coupling of motor activity with ligand-receptor kinetics at adhesion sites. Instead here it emerges as a consequence of the cell boundary satisfying of energy minimization and global geometrical constraint imposed by the theorem of turning tangents. To our knowledge no experimental evidence has yet been put forward of such instabilities. The result can be tested in cell traction assays by varying motor activity in a cycle.

Finally, recent experiments on multicellular systems [26] demonstrated that cohesive cell colonies behave like single cells in their distribution of traction stresses and presence of supracellular actin cables localized to the colony periphery. The Contractile Film Model can be conveniently used to study shapes of strongly coupled cell colonies, where colony surface tension stems from actomyosin contractility as well as strength of cadherins mediating cell-cell adhesions.

MATERIALS AND METHODS

Numerical Simulations. The data shown in Figs. 1 and 3a,b,d have been obtained by numerically minimizing the following discrete version of the energy (1):

$$E_1 = \frac{\sigma}{2} \sum_{i=1}^{N-1} (x_i y_{i+1} - x_{i+1} y_i) + \alpha \sum_{i=1}^{N} \langle s_i \rangle \kappa_i^2 + k_s \sum_{i=1}^{N_A} |\boldsymbol{r}_i - \boldsymbol{r}_{0i}|^2$$
$$(15)$$

where the first term corresponds to the area of the irregular polygon of vertices $\boldsymbol{r}_i = (x_i, y_i)$, with $i = 1 \, 2 \ldots N$, and the third sum represents the energetic contribution of the N_A adhesion points. κ_i is the unsigned curvature at the vertex i: $\kappa_i = |\boldsymbol{t}_i - \boldsymbol{t}_{i-1}|/\langle s_i \rangle$ with $\boldsymbol{t}_i = (\boldsymbol{r}_{i+1} - \boldsymbol{r}_i)/|\boldsymbol{r}_{i+1} - \boldsymbol{r}_i|$ the tangent vector at i and

$\langle s_i \rangle = (s_i + s_{i-1})/2$, with $s_i = |\boldsymbol{r}_{i+1} - \boldsymbol{r}_i|$. The discrete energy (15) was minimized using a standard conjugate gradient algorithm. Using (15) allows a direct comparison between simulations and the analytical results presented in the previous sections. However, for very large substrate stiffness, the discrete curve develops self-intersections and the energy becomes ill-defined. In this regime, it is more convenient to approximate the cell as a simplicial complex consisting of mesh M of equilateral triangles. The edges of the triangles can then be treated as elastic springs of zero rest-length, so that the total energy of the mesh is given by:

$$E_2 = \Sigma \sum_{e \in M} |e|^2 + \alpha \sum_{v \in \partial M} \langle s_v \rangle \kappa_v^2 + k_s \sum_{i=1}^{N_A} |\boldsymbol{r}_i - \boldsymbol{r}_{0i}|^2 \quad (16)$$

where v and e represent respectively the vertices and the edges of the mesh and Σ is a spring constant. If the triangles in the mesh are equilateral, this yields a discrete approximation of the interfacial energy σA, with the spring stiffness proportional to the surface tension: i.e. $\sigma \approx 4\Sigma\sqrt{3}/(2 - B/E)$, where B/E is the ratio between the number of boundary edges B and the total number of edges E of the triangular mesh [21].

[1] D. Discher, P. Janmey, and Y. Wang, Science **310**, 1139 (2005).

[2] T. Yeung, P. Georges, L. Flanagan, B. Marg, M. Ortiz, M. Funaki, N. Zahir, W. Ming, V. Weaver, and P. Janmey, Cell Motil Cytoskel **60**, 24 (2005).

[3] A. Chopra, E. Tabdanov, H. Patel, P. Janmey, and J. Kresh, Am J Physiol-Heart C **300**, H1252 (2011).

[4] C. Chen, M. Mrksich, S. Huang, G. Whitesides, and D. Ingber, Science **276**, 1425 (1997).

[5] C. Galbraith and M. Sheetz, Curr Opin Cell Biol **10**, 566 (1998).

[6] D. Riveline, E. Zamir, N. Balaban, U. Schwarz, T. Ishizaki, S. Narumiya, Z. Kam, B. Geiger, and A. Bershadsky, Science's STKE **153**, 1175 (2001).

[7] R. Bar-Ziv, T. Tlusty, E. Moses, S. Safran, and A. Bershadsky, Proc Natl Acad Sci USA **96**, 10140 (1999).

[8] M. Théry, A. Pépin, E. Dressaire, Y. Chen, and M. Bornens, Cell Motil Cytoskel **63**, 341 (2006).

[9] R. Pelham and Y. Wang, Proc Natl Acad Sci USA **94**, 13661 (1997).

[10] O. Du Roure, A. Saez, A. Buguin, R. Austin, P. Chavrier, P. Siberzan, and B. Ladoux, Proc Natl Acad Sci USA **102**, 2390 (2005).

[11] T. Lecuit and P. Lenne, Nat Rev Mol Cell Bio **8**, 633 (2007).

[12] C. Mader, E. Hinchcliffe, and Y. Wang, Soft Matter **3**, 357 (2007).

[13] R. Buchsbaum, J Cell Sci **120**, 1149 (2007).

[14] M. Wozniak, K. Modzelewska, L. Kwong, and P. Keely, BBA-Mol Cell Res **1692**, 103 (2004).

[15] A. E. H. Love, *A Treatise on the Mathematical Theory of Elasticity*, 4th ed. (Cambridge University Press, Cambridge, 1927).

[16] D. Mumford, in *Algebraic geometry and its applications*, edited by C. Bajaj (Springer-Verlag, New York, 1993) pp. 507–518.

[17] J. Flaherty, J. Keller, and S. Rubinow, SIAM Journal on Applied Mathematics **23**, 446 (1972).

[18] G. Arreaga, R. Capovilla, C. Chryssomalakos, and J. Guven, Phys Rev E **65**, 031801 (2002).

[19] V. Vassilev, P. Djondjorov, and I. Mladenov, J Phys A-Math Gen **41**, 435201 (2008).

[20] P. Djondjorov, V. Vassilev, and I. Mladenov, Int J Mech Sci **53**, 355 (2011).

[21] L. Giomi and L. Mahadevan, Proc R Soc A **468**, 1851 (2012).

[22] I. Bischofs, F. Klein, D. Lehnert, M. Bastmeyer, and U. Schwarz, Biophys J **95**, 3488 (2008).

[23] I. Bischofs, S. Schmidt, and U. Schwarz, Phys Rev Lett **103**, 48101 (2009).

[24] M. Ghibaudo, A. Saez, L. Trichet, A. Xayaphoummine, J. Browaeys, P. Silberzan, A. Buguin, and B. Ladoux, Soft Matter **4**, 1836 (2008).

[25] C. Lemmon, N. Sniadecki, S. Ruiz, J. Tan, L. Romer, and C. Chen, Mechanics & chemistry of biosystems: MCB **2**, 1 (2005).

[26] A. Mertz, S. Banerjee, Y. Che, G. German, Y. Xu, C. Hyland, M. Marchetti, V. Horsley, and E. Dufresne, Phys Rev Lett **108**, 198101 (2012).

[27] G. Charras, M. Coughlin, T. Mitchison, and L. Mahadevan, Biophys J **94**, 1836 (2008).

[28] T. Wakatsuki, R. Wysolmerski, and E. Elson, J Cell Sci **116**, 1617 (2003).

[29] A. Gray, *Modern differential geometry of curves and surfaces with mathematica* (CRC-Press, Boca Raton, FL, 1997).

[30] D. Mitrossilis, J. Fouchard, A. Guiroy, N. Desprat, N. Rodriguez, B. Fabry, and A. Asnacios, Proc Natl Acad Sci USA **106**, 18243 (2009).

[31] S. Banerjee and M. C. Marchetti, Phys Rev Lett **109**, 108101 (2012).